Studies on the Effect of an External Flaw on the Tensile Strength of Short Kevlar Fiber–Thermoplastic Polyurethane Composites

SUNIL K. N. KUTTY* and GOLOK B. NANDO†

Rubber Technology Centre, Indian Institute of Technology, Kharagpur - 721 302, India

SYNOPSIS

The effect of an external flaw on the tensile strength of short kevlar fiber–thermoplastic polyurethane (TPU) composites has been studied with respect to fiber content, fiber orientation, location of the external flaw, and the temperature of test. The composites showed a three-step reduction in tensile strength with increasing flaw size. The critical flaw-length region was shifted to higher flaw-size levels with increasing fiber content. With increasing temperature, the critical flaw length was increased in the case of unfilled TPU, whereas it remained more or less constant in the case of short kevlar fiber-filled–TPU composite.

INTRODUCTION

The presence of flaws both internal and external raises the stress in the vicinity of a flaw, thereby reducing the ultimate strength of the material. According to Inglis,[1] for elastic bodies, the stress amplification due to an edge flaw of length l and tip radius r is

$$\sigma_t/\sigma = 1 + 2\,(l/r)^{1/2} \qquad (1)$$

where σ is the average stress in the material and σ_t is the stress at the tip of the flaw.
When $l \gg r$,

$$\sigma = (\sigma_t \cdot r^{1/2})/2 \cdot l^{1/2} \qquad (2)$$

In other words, the breaking stress varies inversely with the square root of the length of the flaw. Thomas[2] studied the effect of flaws on the tensile strength and fatigue life of natural rubber (NR). Application of flaw growth and critical crack phenomenon to the fatigue failure of NR has been studied extensively.[3–7] The tearing energy criterion and the change in stored energy during the tearing of a rubber held in simple extension and containing a small flaw on one edge were studied by Rivlin and Thomas.[8] The effect of temperature on the tensile strength and critical flaw length of different rubber vulcanizates and glass fiber–epoxy and glass fiber–unsaturated polyester composites have been reported.[9–13] However, studies on the effect of an artificial flaw and its position on the tensile properties of short fiber–elastomer composites are limited.[14]

In an earlier communication, the authors reported the mechanical properties of short kevlar fiber–thermoplastic polyurethane (TPU) composite.[15] The tensile strength gradually increased with fiber content after a minimum at 10 phr fiber content, and elongation at break decreased drastically in the presence of short fibers. Stress relaxation behavior and rheological characteristics of short kevlar–TPU have been reported earlier.[16,17]

In this paper, the results of our studies on the effect of the size and position of external flaws on the tensile strength of short kevlar fiber–TPU composites are reported. The effects of fiber content and temperature on the behavior of the composite to an external flaw have also been studied. The results have further been supplemented by studying the fracture morphology of the failure surfaces with the help of a scanning electron microscope (SEM).

* Present address: Department of Polymer Science and Rubber Technology, Cochin University of Science and Technology, Kochi, India 682 022.

† To whom correspondence should be addressed.

Journal of Applied Polymer Science, Vol. 46, 471–481 (1992)
 CCC 0021-8995/92/030471-11$04.00

Table I Formulation of the Samples

Ingredients	Mix No.				
	K0	K10	K20	K30	K40
TPU[a]	100	100	100	100	100
Kevlar[b]	—	10	20	30	40

[a] Ether-based thermoplastic polyurethane (Estane 58311) from Urethane India Ltd.

[b] Kevlar, aramid short fibers (T-970), from Du Pont de Nemours Co., U.S.A.

Table II Mixing Sequence

Ingredient	Time (min)	rpm	Ram
1/2 TPU	0	30	Up
Fiber	1.5	30	Up
1/2 TPU	3.0	60	Down
—	9.0	—	Dump

EXPERIMENTAL

Materials

Ether-based TPU (Estane 58311, $\bar{M}_W$ = 1.5 E5; T_g determined by DMA = −21°C) was procured from Urethane India Ltd., Madras. Short kevlar staple fiber T-970 (average length = 6 mm and L/D 500 μ) was procured from Du Pont de Nemours Co., U.S.A.

Processing

The formulation of the samples are given in Table I. The mixing of TPU with kevlar fiber was carried out in a Brabender Plasticorder PLE 330 at 180°C and at 60 rpm rotor speed, after drying the ingredients in an air oven at 105°C for 2 h. The mixing sequence is given in Table II. At the end of mixing, the material was sheeted out on a laboratory two-roll open-mixing mill at a nip gap of 0.8 mm so as

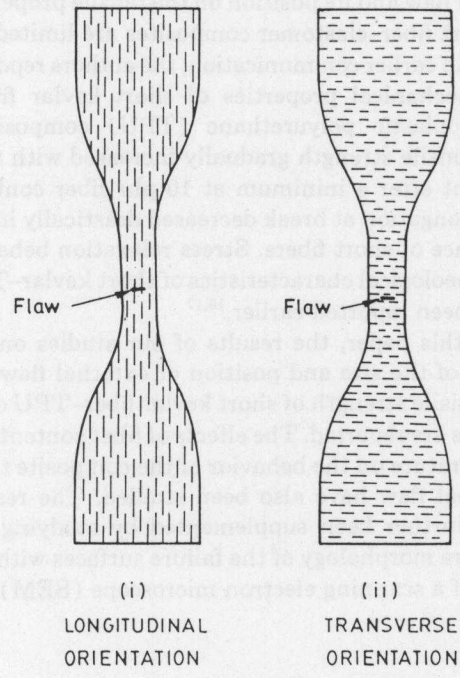

Figure 1 Schematic representation of the orientation of fiber and flaw in the test specimen.

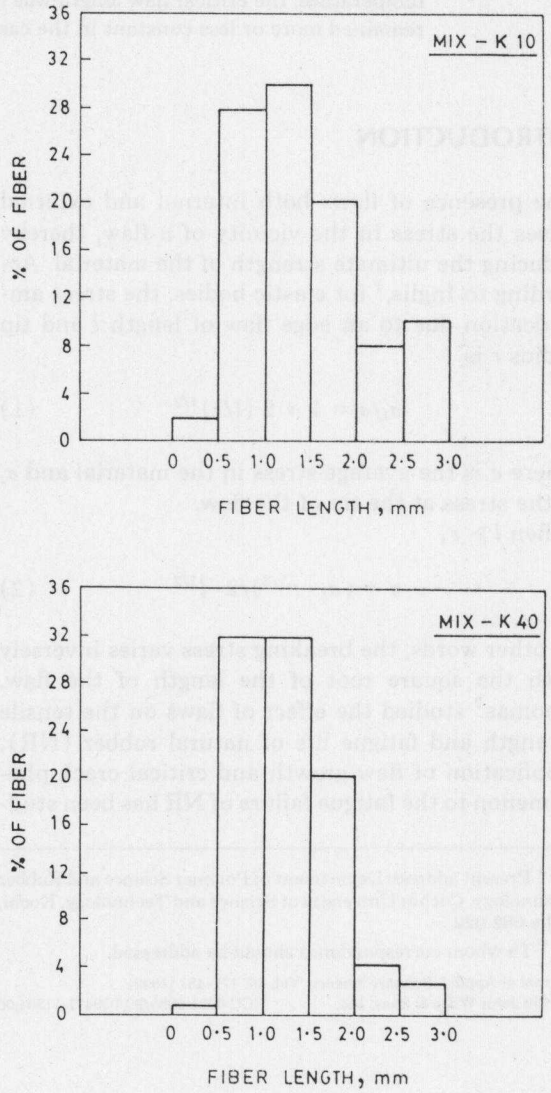

Figure 2 Fiber-length distribution after mixing in samples K10 and K40.

to orient the fibers preferentially in the mill direction. Tensile sheets were molded in a Labo press by heating at 180°C under 45 kg/cm^2 pressure for 3 min and cooling by passing water through the platens. The tensile dumbbells were punched out from these molded sheets with ASTM D Die C. Flaws of different lengths were made in the middle of the specimens by using a special jig attached to chisels of different sizes. Flaws on the side of the specimens were made using a razor blade. Tensile properties were determined on an Instron UTM at a crosshead speed of 500 mm/min. Elevated temperature (50, 75, 100°C) tests were carried out using a temperature cabinet attached to the Instron UTM. A schematic representation of the orientation of the fiber and the external flaw in the test specimens is shown in Figure 1. Fibers were extracted from the molded sheet by dissolving the matrix in tetrahydrofuran and the lengths were measured using a traveling microscope. The distribution of fiber length was calculated from a representative sample of 80–100 fibers. Fractured surfaces of the specimens were studied under an SEM.

RESULTS AND DISCUSSION

Fiber Breakage

Figure 2 gives the fiber-length distribution of samples K10 and K40 after mixing. As is evident from the figure, there is a drastic reduction in length during mixing due to high shear experienced in the Brabender. Average fiber length is reduced from 6 mm to 0.5–1.5 mm after mixing. The breakage takes place through a kinking stage.[15]

Stress–Strain Behavior

Figure 3(a) and (b) gives the stress–strain behavior of the samples K0 and K20, respectively, at 25, 50, 75, and 100°C. The modulus and tensile strength are reduced and elongation at break is increased as the temperature is increased for the unfilled TPU (sample K0), indicating a gradual softening of the matrix. In the presence of 20 phr of fiber [Fig. 3(b)], almost superimposing stress–strain curves at different temperatures indicate that the fiber increases the stiffness of the matrix at elevated temperatures.

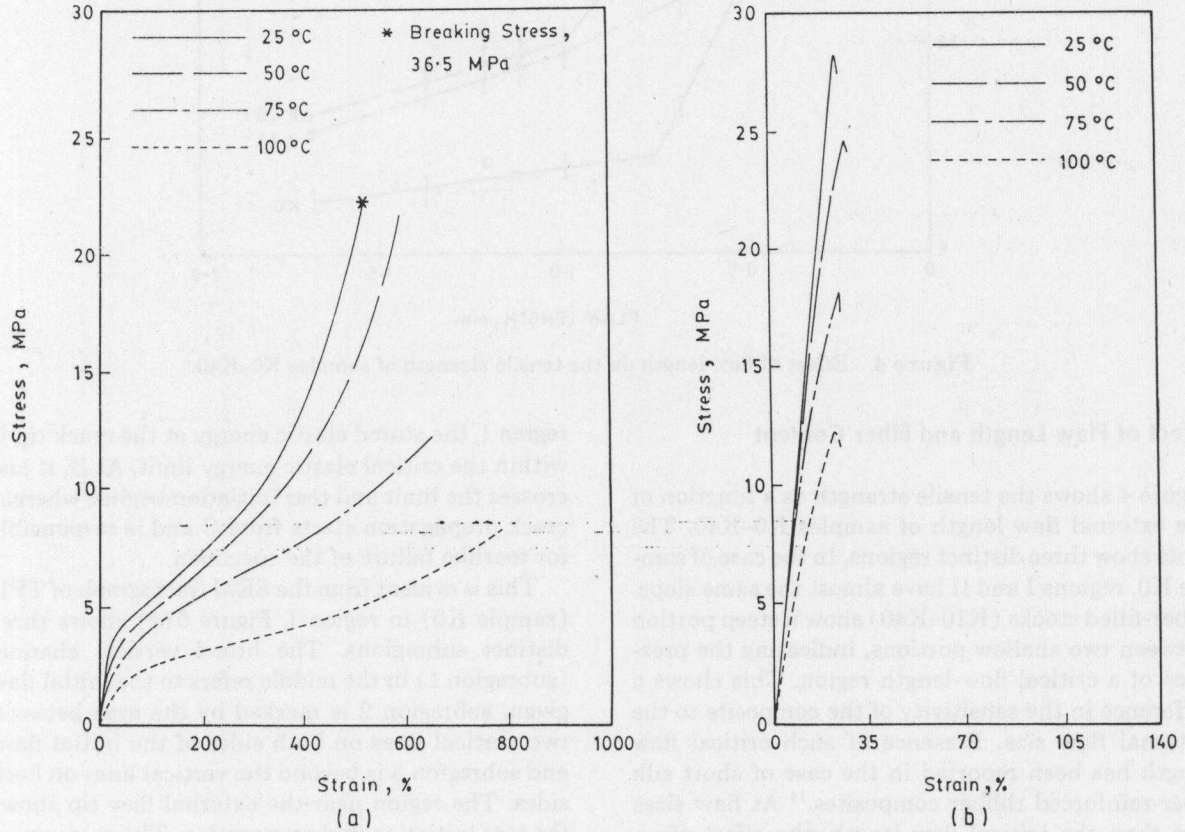

Figure 3 Stress–strain behavior of samples K0 and K20 at different temperatures: (a) sample K0; (b) sample K20.

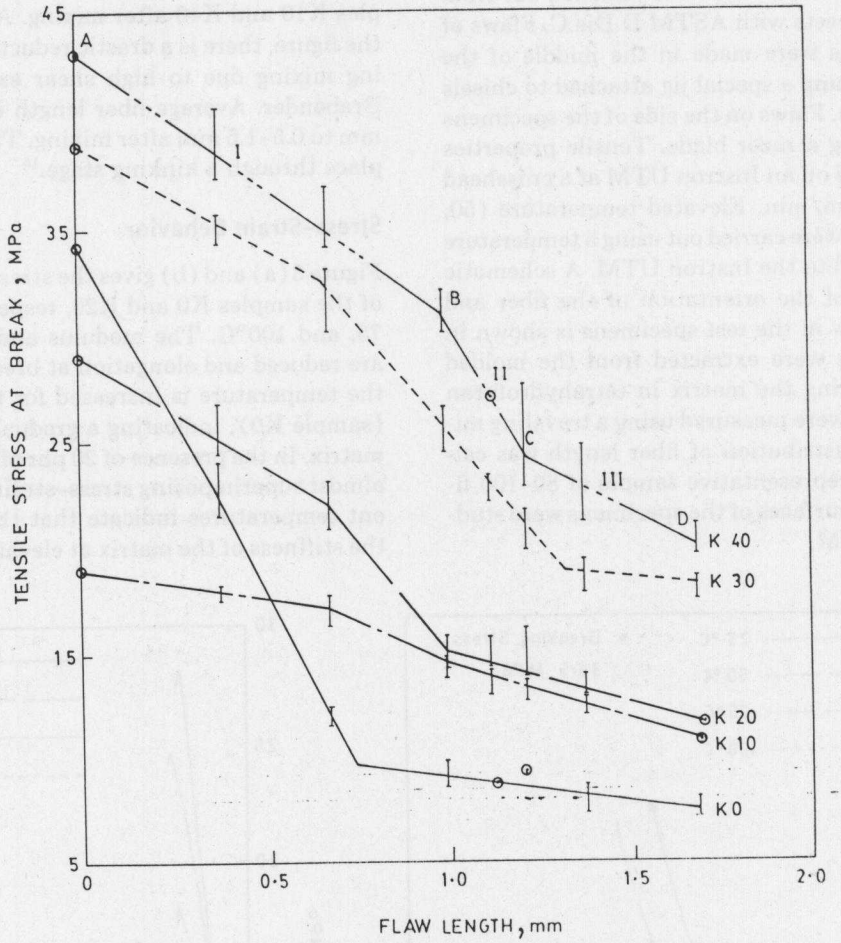

Figure 4 Effect of flaw length on the tensile strength of samples K0–K40.

Effect of Flaw Length and Fiber Content

Figure 4 shows the tensile strength as a function of the external flaw length of samples K0–K40. The plots show three distinct regions. In the case of sample K0, regions I and II have almost the same slope. Fiber-filled stocks (K10–K40) show a steep portion between two shallow portions, indicating the presence of a critical flaw-length region. This shows a difference in the sensitivity of the composite to the external flaw size. Presence of such critical flaw length has been reported in the case of short silk fiber-reinforced rubber composites.[14] At flaw sizes less than the critical flaw length, the effect of an external flaw on the tensile strength is less significant than at the critical flaw-length region. This indicates that in region I the sample failure is due mainly to the material flaws, i.e., the cumulative effect of the material flaws is higher than that of the external flaw. According to Rivlin and Thomas,[8] in region I, the stored elastic energy at the crack tip is within the critical elastic energy limit. At B, it just crosses the limit and tear initiation begins, whereas crack propagation starts from C and is responsible for tearlike failure of the specimen.

This is evident from the SEM fractograph of TPU (sample K0) in region I. Figure 5(a) shows three distinct subregions. The broad vertical channel (subregion 1) in the middle refers to the initial flaw given, subregion 2 is marked by the area between two vertical lines on both sides of the initial flaw, and subregion 3 is beyond the vertical lines on both sides. The region near the external flaw tip shows the tear initiation and propagation. The presence of a larger number of tear lines points to a highly strained state of matrix near the crack tip. According to strain amplification theory, even though the overall elongation is very low in a bulk deformation, the local strain may be of the order of the breaking strain. This may lead to local strain-induced crys-

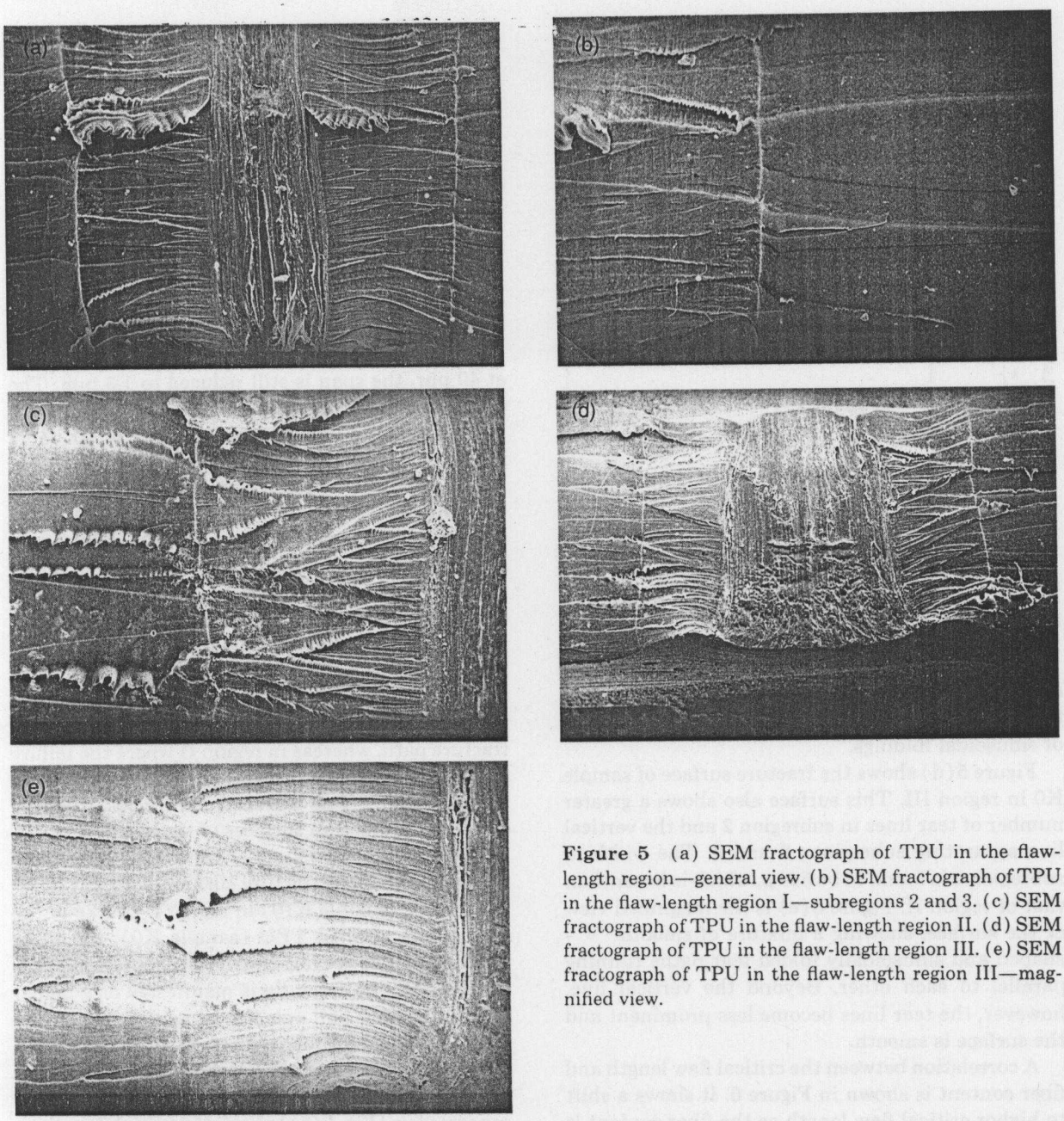

Figure 5 (a) SEM fractograph of TPU in the flaw-length region—general view. (b) SEM fractograph of TPU in the flaw-length region I—subregions 2 and 3. (c) SEM fractograph of TPU in the flaw-length region II. (d) SEM fractograph of TPU in the flaw-length region III. (e) SEM fractograph of TPU in the flaw-length region III—magnified view.

tallization near the crack tip and formation of microfolds at the fracture surface. This region is clearly seen in Figure 5(a). At a definite distance from the crack tip, the different tear lines tend to merge, forming a "V"-shaped tear path and two vertical lines on both sides of the initial flaw. The formation of this vertical line across the tear path is attributed to the momentary halt of the tearing because of relaxation of the stored strain energy at the external flaw tip during the tear propagation. The distance between this line and the flaw edge is about 540 μ. Subregion 3 is characterized by a comparatively smooth surface, indicating a smooth propagation of tear. Figure 5(b) shows region 2 at the left and subregion 3 at the right of the vertical line.

The SEM fractograph of sample K0 in region II [Fig. 5(c)] also shows three subregions. The vertical lines parallel to the flaw edge occur at a distance of 640 μ. Notable features of this fracture surface are (a) the presence of a comparatively larger number

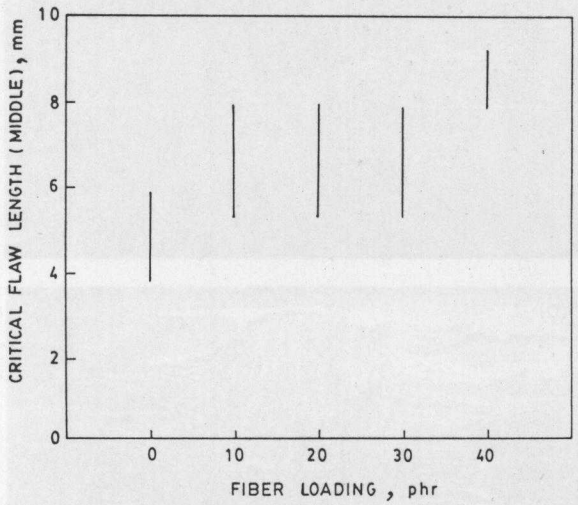

Figure 6 Effect of fiber content on the critical flaw length.

of tear lines originating at the crack tip and (b) that the tear paths propagate across the width in the form of sinusoidal foldings.

Figure 5(d) shows the fracture surface of sample K0 in region III. This surface also shows a greater number of tear lines in subregion 2 and the vertical line separating subregions 2 and 3. The width of subregion 2 is found to be 580 μ, which is lower than that of region II. Figure 5(e) is the magnified view of the surface, showing a mixture of smooth "V"-shaped and sinusoidally folded tear paths running parallel to each other. Beyond the vertical line, however, the tear lines become less prominent and the surface is smooth.

A correlation between the critical flaw length and fiber content is shown in Figure 6. It shows a shift to higher critical flaw length as the fiber content is increased from 10 to 40 phr. At fiber contents of 10–30 phr, the shift occurs by about 1.25 mm, and at 40 phr, the value is further shifted to higher levels. This can be explained as due to the hindrance given by the fibers to the advancing fracture front.

The length of the critical flaw-length regions and the slopes of different regions of the tensile strength–flaw size plot (Fig. 4) are given in Table III. The range of critical flaw length is reduced from 3 to 2.5 mm in the presence of short fibers up to 20 phr, and at 40 phr, the span is still reduced to 1.3 mm. The slopes of regions I and II are found to decrease with fiber content. At 10 phr content of short fibers, there is a drastic reduction in the slopes of regions I and II (91 and 76%, respectively). For fiber content in the range 20–30 phr, the reduction is 67–70% in the case of region I and 38–40% in the case of region II. At 40 phr fiber content, the corresponding values are 61 and 16%. In other words, the rate of the fall of tensile strength with respect to flaw size is reduced in the presence of short fibers for shorter flaw sizes. This is because in region I the failure is initiated at natural flaws and the fibers, distributed uniformly in the matrix, can deflect or arrest the propagating fracture path, whereas in region II where the failure starts at the external flaw tip, the effect of fiber is less significant. This has been confirmed further by the study of fracture surfaces of the samples in different flaw-length regions. Figure 7(a) shows the general view of the fracture surface of 10 phr fiber-filled stock (sample K10) in region I. Unlike in the case of the unfilled TPU (sample K0), the three distinct regions are not clearly seen. Stress concentration near the crack tip is manifested as a higher amount of fiber pull out. Focusing at the crack tip shows [Fig. 7(b)] fiber pullout holes, broken fiber, and tear lines starting at the crack tip. In region II also, the fracture surface shows only two regions. A general view [Fig. 7(c)] shows the initial flaw given and the broken fiber ends and pullout holes.

At all fiber content, slope III is found to be higher

Table III Critical Flaw-Length Characteristics of Samples K0–K40

Mix	Length at B (mm)	Length at C (mm)	Critical Flaw Length (mm)	Slope I (of AB)	Slope II (of BC)	Slope III (of CD)
K0	2.90	5.9	3.00	32.7	36.4	2.7
K10	5.35	7.9	2.55	2.8	8.7	5.6
K20	5.35	7.9	2.55	10.7	22.7	5.1
K30	5.30	7.7	2.40	9.8	21.9	5.0
K40	7.90	9.2	1.30	12.9	30.7	9.6
K20(T)[a]	—	8.0	8.00	9.9	9.9	5.1

[a] Mix K20 with the fibers oriented in the transverse direction.

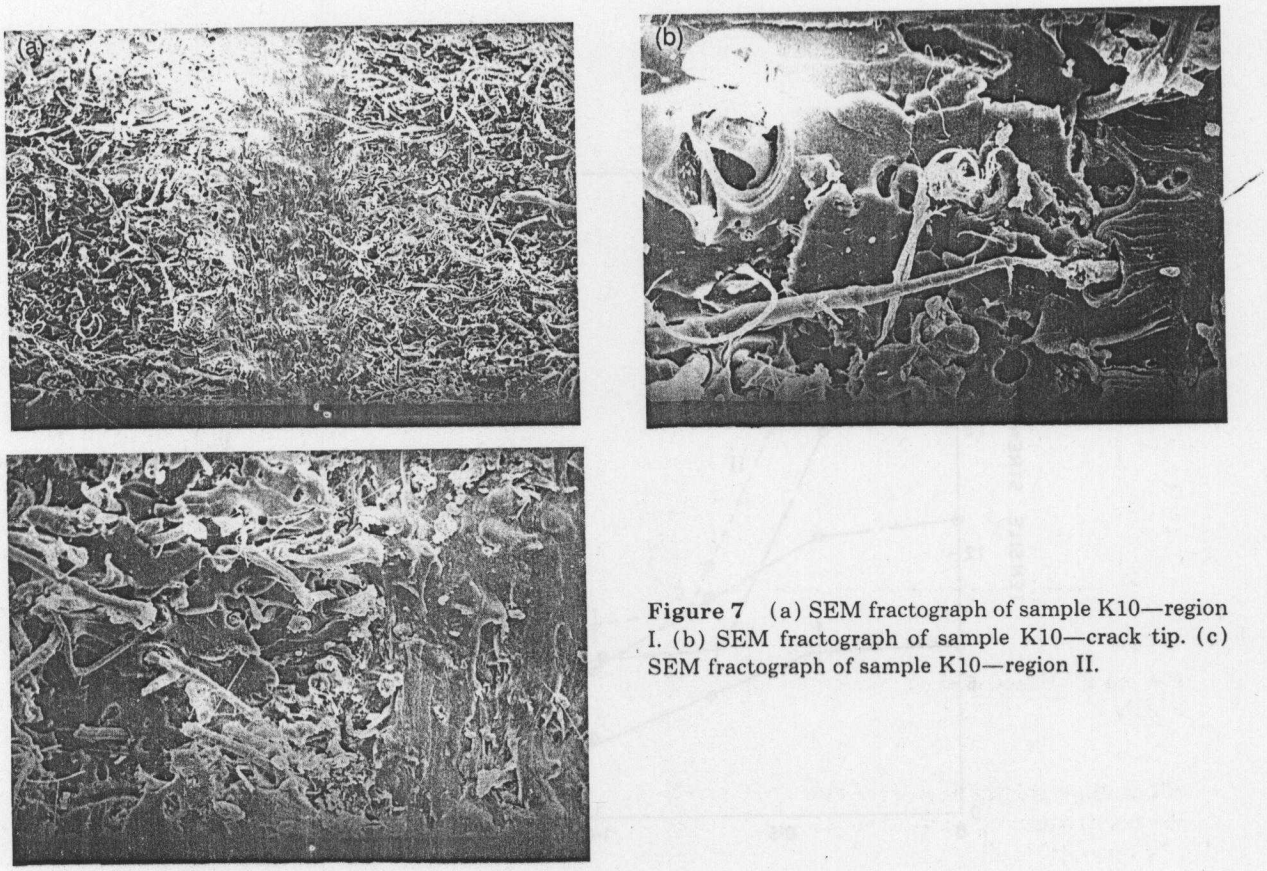

Figure 7 (a) SEM fractograph of sample K10—region I. (b) SEM fractograph of sample K10—crack tip. (c) SEM fractograph of sample K10—region II.

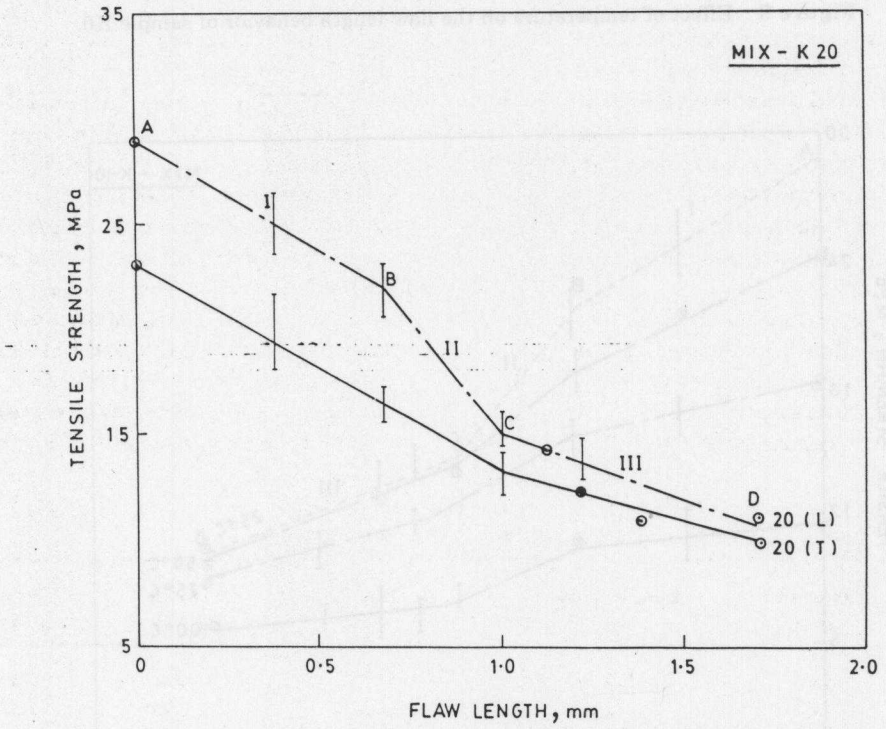

Figure 8 Effect of fiber orientation on the flaw-length behavior of sample K20.

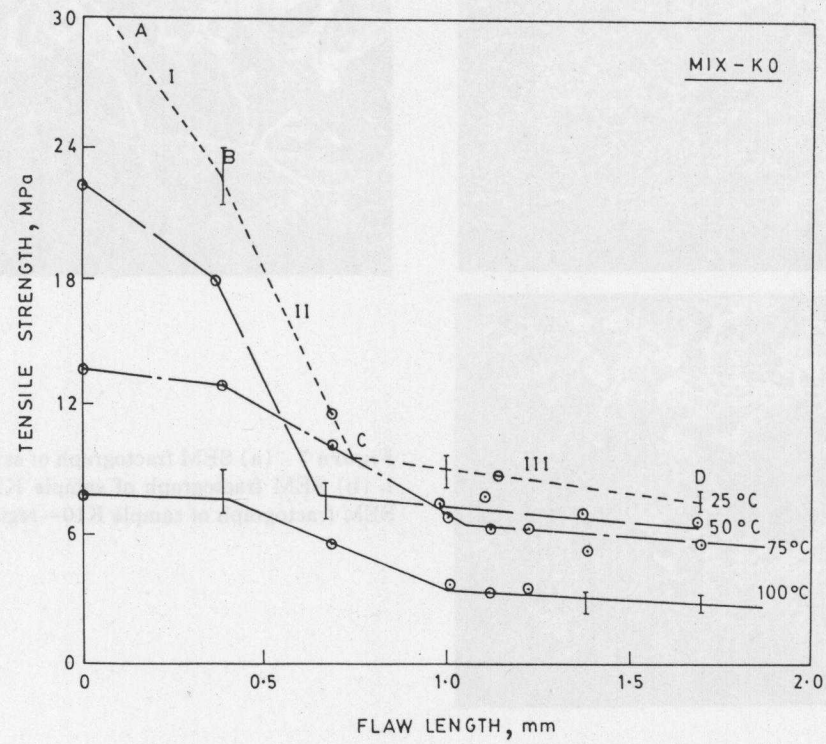

Figure 9 Effect of temperature on the flaw-length behavior of sample K0.

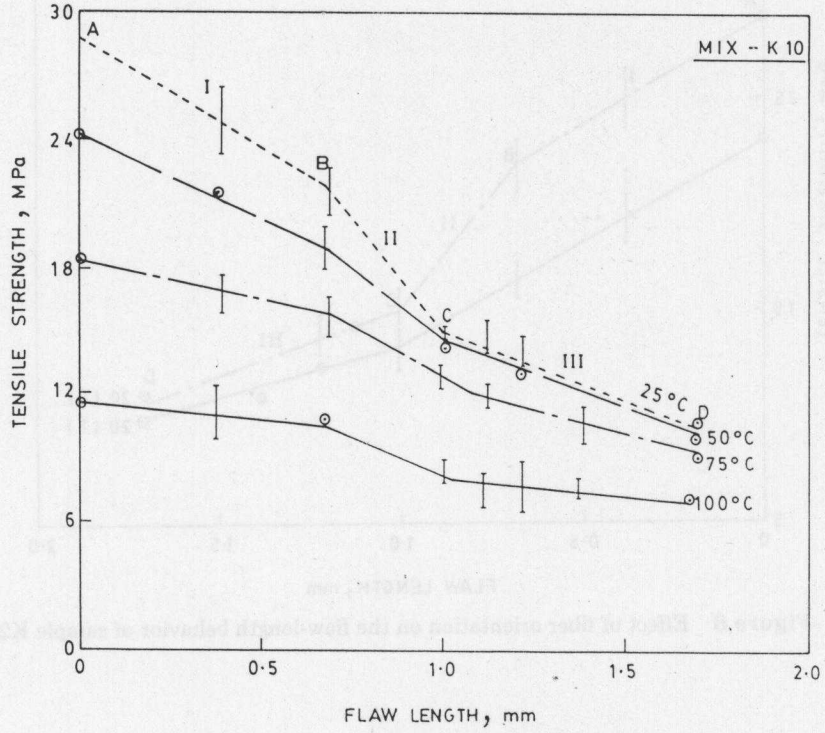

Figure 10 Effect of temperature on the flaw-length behavior of sample K20.

Table IV Critical Flaw-Length Characteristics of Samples K0 and K20 at Different Temperatures

Mix	Temperature (°C)	Length at B (mm)	Length at C (mm)	Critical Flaw Length (mm)	Slope I (of AB)	Slope II (of BC)	Slope III (of CD)
K0	25	3.0	5.8	2.8	24.4	38.1	2.5
K0	50	2.9	5.1	2.2	12.4	38.1	1.7
K0	75	3.0	8.3	5.3	2.2	10.3	1.6
K0	100	3.1	7.9	4.8	0.8	7.4	1.2
K20	25	5.4	7.9	2.6	11.1	23.1	6.8
K20	50	5.4	8.0	2.6	8.3	14.1	6.6
K20	75	5.4	8.5	3.1	3.9	10.3	4.9
K20	100	5.4	8.1	2.8	2.0	7.9	2.0

than that of sample K0. This is because as the external flaw size increases the fibers are no longer effective in arresting the fracture front; rather, they act as stress raisers.

Effect of Orientation of Fiber

Figure 8 shows the flaw-length behavior of sample K20 with fibers oriented preferentially in two directions—longitudinal and transverse (see Fig. 1). The effect of change in fiber orientation is clearly manifested in the lower flaw-length ranges. In the transverse direction where the fibers are parallel to the direction of the propagation of the fracture, the tear propagates unhindered and, hence, the behavior is similar to that of the gum compound, whereas in the case of longitudinal orientation of fibers, three distinct regions are observed.

Effect of Temperature

Figures 9 and 10 show the flaw-length behavior of samples K0 and K20 at four different temperatures. The different points of inflection and slopes are given in Table IV. In the case of sample K0, as the temperature is increased, two points become apparent: (i) the slope of the region AB is reduced, and (ii) the region BC is spread over a wider range and the slope is reduced. The region CD is similar at all temperatures studied. Point B remains independent of the temperature within the temperature studied, whereas point C is shifted to a higher flaw-size level at 75 and 100°C. Critical flaw length also is increased at temperatures above 50°C by approximately 80%. In the case of sample K20, the critical flaw length remains more or less constant. Slope I is reduced drastically as the temperature is raised. The reduction is about 97% for a temperature rise of 75°C from 25°C, whereas for the fiber-filled stocks, the reduction is 82% for the same temperature rise. Slope II is reduced from 38 to 7.4 for sample K0 and 23 to 7.9 for sample K20. Slope III is also reduced with an increase in temperature. Because the matrix becomes weak as the temperature is increased, the crack propagation starts at a lower level of stored strain energy, resulting in lower ultimate strength.

Slopes of regions I, II, and III were plotted against the inverse of temperature in semilog scale and the activation energies were calculated using the following equation for samples K0 and K20 (Table V):

$$\ln K_r = A - E_a/(RT)$$

where T is temperature in Kelvin; R, the gas constant, cal mol^{-1} K^{-1}; A, the preexponential factor; and E_a, the activation energy, kcal mol^{-1}. It shows a definite temperature dependence of the process. The presence of fibers reduces the activation energy by 50% for regions I and II. However, for region III, the activation energy is found to be greater in the presence of 20 phr of fibers.

Table V Activation Energies Calculated at Different Regions

	Activation Energy (kcal mol^{-1})		
Mix	Slope I	Slope II	Slope III
K0	10.5	5.4	2.0
K20	5.1	3.1	3.4

Effect of Side Flaw

According to eq. (2), the breaking strength in the case of samples with a side flaw will vary as a function of flaw length. Plotting the breaking strength as a function of the size of the side flaw of samples K0 and K20 (Figs. 11 and 12), the strength decreases asymptotically as predicted earlier by Thomas.[2] On extrapolation to the breaking strength of the uncut

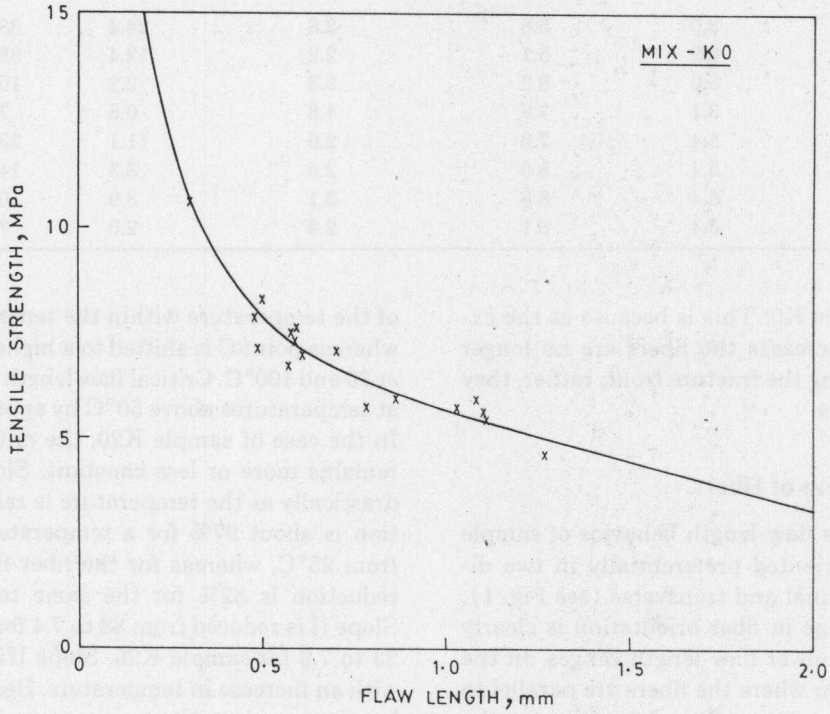

Figure 11 Effect of side flaw on the tensile strength of sample K0.

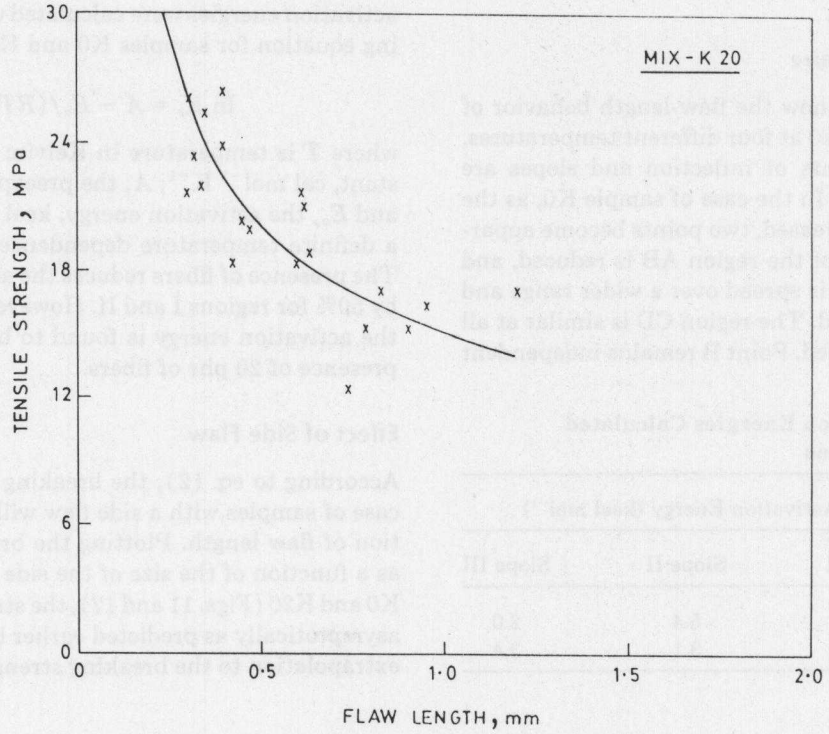

Figure 12 Effect of side flaw on the tensile strength of sample K20.

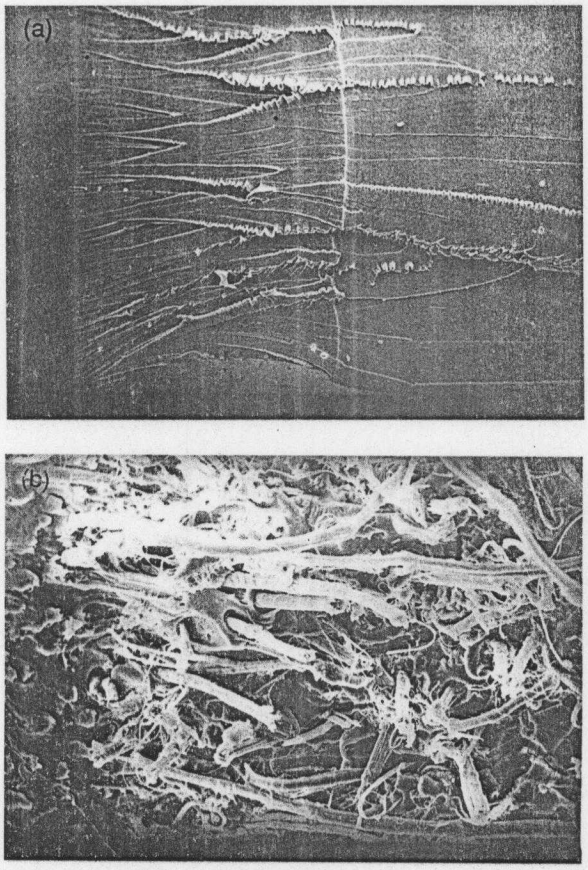

Figure 13 (a) SEM fractograph of TPU—external flaw on one edge. (b) SEM fractograph of sample K20—external flaw on one edge.

sample, a flaw size of 0.22 mm is obtained for sample K0. For sample K20, the value of the flaw size obtained is 0.27 mm. According to Gent,[18] this characteristic value is independent of the particular elastomer or sample formulation used.

SEM study of the side-flaw samples revealed three distinct regions as in the case of middle-flaw samples [Fig. 13(a)]. The fracture lines are seen originating at the external crack tip at the left and then propagate to the right. The lines on magnification show sinusoidal foldings in a "V"-shaped tear path. The vertical line that separates subregions 2 and 3 is at a distance of about 970 μ, a value much higher than that of the middle-flaw samples. The higher-strain amplification due to a lower crack tip radius in this (as the flaw was made with razor blade) justifies the observation. Subregion 3 is comparatively smoother in this case with occasional knotty tear lines. In the case of the 20 phr fiber-filled sample, all the three subregions again are not visible [Fig. 13(b)].

CONCLUSIONS

From the above study, the following conclusions have been drawn:

1. A critical flaw-length region through which the tensile strength falls drastically with increasing external flaw size exists in the case of TPU and short kevlar fiber–TPU composite.
2. The rate of fall of tensile strength with respect to flaw size is reduced in the presence of short fibers for shorter flaw sizes.
3. With increasing temperature from 25 to 100°C, the critical flaw-length region of neat TPU is increased by 80%, whereas it remains independent of temperature in the presence of 20 phr of the short kevlar fiber.

REFERENCES

1. C. E. Inglis, *Trans. Inst. Nav. Archit.*, **55,** 219 (1913).
2. A. G. Thomas, *Rubb. Chem. Technol.*, **48,** 5 (1975).
3. A. N. Gent, P. B. Lindley, and A. G. Thomas, *J. Appl. Polym. Sci.*, **8,** 455 (1964).
4. K. Fujimoto and T. Migita, *Nippon Gommu Kyokaishi,* **12,** 730 (1980).
5. K. Fujimoto, T. Migita, and K. Suzuki, *Nippon Gomu Kyokaishi,* **1,** 53 (1981).
6. A. G. Thomas, *J. Polym. Sci.*, **31,** 467 (1958).
7. A. Stevenson, *Int. J. Fracture,* **23,** 47 (1983).
8. R. S. Rivlin and A. G. Thomas, *J. Polym. Sci.*, **10,** 291 (1953).
9. B. S. T. T. Boonstra, *India Rubb. World,* **121,** 299 (1949).
10. S. Kose, *J. Polym. Sci.*, **11,** 425 (1953).
11. A. G. Thomas and J. M. Whittle, *Rubb. Chem. Technol.*, **43,** 222 (1970).
12. C. L. M. Bell, D. Stinson, and A. G. Thomas, *Rubb. Chem. Technol.*, **55,** 66 (1982).
13. M. Miwa, A. Nakayama, T. Ohsawa, and A. Hasegawa, *J. Appl. Polym. Sci.*, **23,** 2957 (1979).
14. D. K. Setua and S. K. De, *J. Mater. Sci.*, **20,** 2653 (1985).
15. S. K. N. Kutty and G. B. Nando, *J. Appl. Polym. Sci.*, to appear.
16. S. K. N. Kutty and G. B. Nando, *J. Appl. Polym. Sci.*, **42,** 1835 (1991).
17. S. K. N. Kutty, P. P. De, and G. B. Nando, *Plast. Rubber Compos. Proc. Appl.*, **15**(1), 23 (1991).
18. A. N. Gent, in *Strength of Elastomers in Science and Technology of Rubber,* F. R. Eirich, Ed., Academic Press Orlando, FL, 1978, p. 419.

Received July 9, 1991
Accepted November 11, 1991